Journal of Molecular Catalysis A: Chemical 308 (2009) 150–158

Contents lists available at ScienceDirect

Journal of Molecular Catalysis A: Chemical

journal homepage: www.elsevier.com/locate/molcata

Synthesis, characterization and catalytic performance of vanadia-doped delaminated zirconia-pillared montmorillonite clay for the selective catalytic oxidation of hydrogen sulfide

Kanattukara Vijayan Bineesh, Sang-Yun Kim, Balasamy Rabindran Jermy, Dae-Won Park*

Division of Chemical Engineering, Pusan National University, Busan 609-735, Republic of Korea

ARTICLE INFO

Article history:
Received 6 December 2008
Received in revised form 1 April 2009
Accepted 2 April 2009
Available online 10 April 2009

Keywords:
Pillared-clay
Delamination
Selective catalytic oxidation
Hydrogen sulfide

ABSTRACT

A series of vanadia-doped zirconia-pillared clays (V/Zr-PILCs) with various amounts of vanadia were prepared and their performance for the selective catalytic oxidation of H_2S was investigated in this study. V/Zr-PILCs were characterized using X-ray diffraction (XRD), surface area-pore volume measurements, chemical analysis, X-ray photoelectron spectroscopy (XPS), ^{51}V spin-echo NMR, temperature-programmed reduction by H_2 (H_2-TPR) and temperature-programmed desorption of ammonia (NH_3-TPD). V/Zr-PILCs showed better catalytic performance than as such Zr-PILC at temperatures ranging from 220 to 300 °C without any considerable SO_2 emission. The H_2S conversion over V/Zr-PILCs increased with increasing vanadia content up to 6 wt.%. This superior catalytic performance might be related to the uniform dispersion of vanadia in the form of monomeric and polymeric species. However, it decreased at higher vanadia loadings due to the decrease of surface area and to the formation of crystalline V_2O_5 phase. The presence of water vapor in the reactant mixture resulted in the decrease of the H_2S conversion.

© 2009 Elsevier B.V. All rights reserved.

1. Introduction

Since international environmental regulations concerning the release of sulfur-containing gas have become more stringent, hydrogen sulfide contained in acidic gases needs to be carefully controlled prior to emission to the atmosphere. For many years, most hydrogen sulfide in petroleum refineries and natural gas plants has been removed using the well-known Claus process [1,2]. However, due to thermodynamic limitations, 3–5% of the H_2S is not converted to sulfur. Various commercial processes based on adsorption, absorption, and wet oxidation have been used to treat the tail gas having low concentration (<5 vol.%) of sulfur-containing gas from the Claus plant or other emission sources. Among these processes, the most attractive process is the dry catalytic oxidation of H_2S to elemental sulfur after the hydrogenation of sulfur-containing gas to H_2S. Two important commercial developed processes are the MODOP (Mobil direct oxidation) process [3,4] and Super Claus process [1,5]. These processes are based on the following irreversible selective oxidation of H_2S to S (reaction (1)) as the main reaction, with other oxidation reactions (reactions (2) and (3)) and the reversible Claus reaction (reaction (4) as side reactions.

$$H_2S + (1/2)O_2 \rightarrow (1/n)S_n + H_2O \quad (1)$$

$$(1/n)S_n + O_2 \rightarrow SO_2 \quad (2)$$

$$H_2S + (3/2)O_2 \rightarrow SO_2 + H_2O \quad (3)$$

$$2H_2S + SO_2 \leftrightarrow (3/n)S_n + 2H_2O \quad (4)$$

Clays are unbiquitous and cheap. Clays are now widely used as catalyst due to its eco-friendly nature, but its efficient use is limited due to lack of porosity and low thermal stability. Therefore modifications are done to improve the properties among which pillaring process provide porosity and thermal stability. Pillared interlayered clays (PILCs) are two-dimensional zeolite-like materials that are prepared by exchanging the charge-compensating cations between the clay layers with large inorganic cations, which are polymeric or oligomeric hydroxy metal cations, formed by the hydrolysis of metal oxides or metal salts. Upon heating, the metal hydroxy cations undergo dehydration and dehydroxylation, forming stable metal oxide clusters that act as pillars that maintain separation between the silicate layers and create interlayer space of molecular dimensions [6–9]. Compared with zeolites, PILCs have the advantage that new materials can be tailored to particular applications by varying the size and separation of the pillars as well as their composition. A wide variety of factors can influence the intercalation/pillaring process, which makes it difficult to compare the results reported by other authors. These factors include the nature of the host clay used as the parent material, nature of the metallic cation, hydrolysis

* Corresponding author. Tel.: +82 51 510 2399; fax: +82 51 512 8563.
E-mail address: dwpark@pusan.ac.kr (D.-W. Park).

1381-1169/$ – see front matter © 2009 Elsevier B.V. All rights reserved.
doi:10.1016/j.molcata.2009.04.002

conditions, reaction time, synthesis temperature, and the washing, drying and calcination processes.

Delaminated pillared clay is one class of pillared clay, which was first synthesized by Pinnavaia et al. [10]. Delaminated clays are solids supports and catalysts characterized by a house-of-card like structure containing, mesopores and macropores, in addition to micropores of the type found in zeolites and pillared clays [11]. The different porosity characteristics of delaminated pillared clays compared to pillared clays will influence their catalytic and adsorption properties. The intercalation of clays with zirconium oligomers has been reported by several authors [12–19].

Several studies have also reported [20–26] the selective catalytic oxidation of H_2S using a variety of catalysts. In our previous work [27,28], we reported the good catalytic performance of V_2O_5 catalyst for the selective oxidation of H_2S. To the best of our knowledge, we are reporting for the first time the selective catalytic oxidation of H_2S using vanadia-doped delaminated zirconia-pillared clay.

2. Experimental

2.1. Catalyst synthesis

The starting material was Na-montmorillonite (Kunipia-F, Kunimine Industrial Company) with a cation exchange capacity of 120 meq/100 g, and is referred to as Na-MMT. Zirconium oxychloride (98%, Sigma-Aldrich) is used as a source of zirconium polycations. $ZrOCl_2{\cdot}8H_2O$ (0.1 M) solution was prepared by dissolving the required amount of the salt in double distilled water. The solution was then refluxed at 100 °C for 24 h to prepare the pillaring solutions. The pillaring processes were performed with 1 wt.% clay slurry. The pillaring solutions were then added drop wise to the aqueous clay suspension under stirring conditions to obtain a final Zr/clay ratio of 10 mmol/g. The slurry was kept under stirring for 24 h at room temperature. After aging for 12 h, the product was filtered, washed several times with distilled water, dried in air and then calcined at 400 °C for 3 h. The final product is referred to as Zr-PILC.

Vanadia loaded Zr-PILC containing 2, 6, 11 and 14 wt.% vanadia were prepared by the wet impregnation of the Zr-PILC support with a solution of NH_4VO_3 (99%, Aldrich) dissolved in water acidified by oxalic acid. The pH during the impregnation process was 2.1. Finally all the samples were dried at 80 °C for 20 h and calcined at 400 °C for 3 h under an air flow. The samples are labeled as *x* wt.% V/Zr-PILC, where *x* refers to the vanadia loading on the support.

2.2. Characterization of the catalysts

The chemical composition of the samples was determined by X-ray fluorescence spectroscopy (XRF, Philips PW 2400).

The X-ray diffraction (XRD) patterns were obtained on a Bruker Advanced D8 powder diffractometer, using Ni filtered Cu Kα radiation (λ = 1.5404 Å). A fixed power source (40 kV, 300 mA), and a scan speed of 0.02° 2θ min^{-1} were applied for the determination of XRD.

The surface areas were determined by N_2 adsorption at 77 K using a Micromeritics ASAP 2010 instrument. The samples were outgassed in vaccum for 12 h at 110 °C prior to nitrogen adsorption. The specific surface areas were calculated using BET equation. The total pore volumes were evaluated from the nitrogen uptake at a relative N_2 pressure of $P/P_0 = 0.99$. The *t*-plot method was used to determine the micropore volume.

XPS analyses were performed using a X-ray photoelectron spectrometer (VG, ESCALAB 250) with monochromatic Al Kα radiation ($h\upsilon$ = 1486.6 eV). Samples calcined at 400 °C for 3 h were pressed into self-supporting wafers without a binder, followed by a pretreatment in an ultrahigh vacuum. The binding energies (BE) were calculated using the C 1s band as the reference (284.6 eV).

The ^{51}V spin-echo NMR spectra were obtained on a Bruker DSX 400 spectrometer (υ_0 = 105.2 MHz for ^{51}V resonance) with a field strength of 9.4 T. All chemical shifts were referenced to $NaVO_3$ as the external standard.

Temperature-programmed reduction by H_2 (H_2-TPR) and temperature-programmed desorption of ammonia (NH_3-TPD) were performed with a BEL-CAT chemisorption apparatus (BEL, JAPAN). For H_2-TPR, about 50 mg of sample was pretreated in an oxidative atmosphere (5% O_2 in He) at 400 °C for 30 min. After cooling to room temperature, the TPR by H_2 (5% in He, flow rate 20 mL/min) was carried out from 100 to 700 °C at a heating rate of 10 °C/min. For NH_3-TPD, about 50 mg of the sample was pretreated to 400 °C for 2 h under He flow, and cooled to ambient temperature. Pure ammonia gas (50 mL/min) was adsorbed at 100 °C for 20 min. Desorption was carried out with a linear heating rate of 10 °C/min in a flow of He (20 mL/min).

2.3. Reaction tests

The reaction tests were carried out in a continuous flow fixed-bed reactor made from Pyrex tube with 1 in. internal diameter. The gas flow rate was controlled using mass flow controllers (Brooks MFC, 5850E). A mixture of gases H_2S, O_2 and a balance of He with purity of 50%, 98%, 99.999%, respectively were used. A sulfur condenser was attached at the effluent side of the reactor and its temperature was maintained at 110 °C to allow the condensation of sulfur vapor only. A line filter was installed after the condenser to trap any sulfur mist that had not been captured by the condenser. From the condenser up to the gas chromatograph, all the lines and fittings were heated to above 120 °C in order to prevent condensation of water vapor. In a typical experiment, the reactant composition consisted of 5 vol.% H_2S, 2.5 vol.% O_2 and a balance of He. The gas hourly space velocity (GHSV) was fixed to 10,000 h^{-1}. Typically, 0.4 g of catalyst was used with total gas flow rate of 100 mL/min. Water vapor was introduced to the reactant stream using a steam evaporator filled with small glass beads, and its amount was controlled using a syringe pump. Before the measurement of catalytic activity, the catalyst was pretreated at 300 °C for 2 h.

The O_2, H_2S and SO_2 content of the effluent gas were analyzed by a gas chromatography (HP 5890) equipped with a thermal conductivity detector and a 1.8 m Porapak T column (80–100 mesh) at 100 °C. The exit gas from the analyzer was passed through a trap containing a concentrated NaOH solution and vented out to a hood. The reproducibility of the conversion results was within the range of ±1.1% and that of the product selectivity was within the range of ±1.3%.

3. Results and discussion

3.1. Chemical composition

Table 1 shows the chemical compositions of the initial clay, Zr-PILC and V/Zr-PILCs. The pillaring of the initial clay by ZrO_2 resulted in an increase in the ZrO_2 content with complete replacement of the interlayer Na cations. The relative amounts of silica, aluminum and magnesium remained constant in all samples after pillaring. This suggests that the compositon of the clay sheet is preserved in Zr-PILC and V/Zr-PILCs. A slight decrease in the ZrO_2 content was observed after the impregnation of vanadia over Zr-PILC.

Table 1
Chemical composition (wt.%) of the samples investigated.

Samples	SiO_2	Al_2O_3	ZrO_2	Na_2O	Fe_2O_3	MgO	V_2O_5
Na-MMT	56.68	29.20	0.12	4.51	2.24	5.84	–
Zr-PILC	33.42	21.35	39.26	≪	0.94	3.95	–
2 wt.% V/Zr-PILC	32.30	20.50	38.22	≪	0.92	3.92	2.31
6 wt.% V/Zr-PILC	31.02	19.12	37.10	≪	0.91	3.73	6.12
11 wt.% V/Zr-PILC	31.53	19.23	30.21	≪	0.91	3.91	11.22
14 wt.% V/Zr-PILC	31.38	18.92	28.42	≪	0.92	3.82	13.64

≪: less than 0.001 wt.%.

3.2. X-ray diffraction

Since the samples used were randomly oriented powder, the X-ray powder diffraction patterns showing the basal (0 0 1) reflection is considered as one of the main identification source for the clay group. Fig. 1 shows the low-angle XRD patterns of the Zr-PILC and V/Zr-PILCs calcined at 400 °C and for the original Na-MMT. Na-MMT shows a main peak at approximately 2θ of 7°, which is commonly assigned to the basal (0 0 1) reflection (d(0 0 1)). In Zr-PILC, the d(0 0 1) peak was found to shift towards a lower 2θ indicating expansion in the layer structure, as a result of pillaring. A diffraction peak of (0 0 1) reflection of Na-MMT was found to be totally absent in pillared clay sample. This proves that zirconia pillars are well distributed in the clay without any contribution due to unpillared portion in the product obtained. The d-spacing of the Zr-PILC calcined at 400 °C was found to be of 46 Å. This d-spacing of Zr-PILC is obviously larger than earlier reports [13–19,29–33]. These results differ markedly, which may be due to the difference in the clay materials used, to the pillaring method or to the other steps of the synthesis procedures. It was reported that when the zirconium solution is refluxed prior to exchange step the basal spacing increases slightly with a decrease in intensity [14,33]. The observed intensity and broadness of the (0 0 1) diffraction peaks show an inhomogeneous stacking of the clay layers, typical of the Zr-PILCs [34–36]. Thus the long range face-to-face association, which is characteristic of the clays, is no longer present and the clay has delaminated during the pillaring process. The presence of short-range layer stacking accounts for the very diffuse (0 0 1) X-ray reflection. Moreover, similar to other reports [37–39], the Zr-containing oligomeric solutions in our synthesis conditions (low pH) also provoke arrangements in the clay structure giving a possible delamination to the clay structure.

High d-spacing in the XRD patterns for other PILCs have been already reported by several authors. Mandalia et al. [40] observed a d-spacing of 72 Å in the XRD pattern of Fe_2O_3-pillared clay. Bergaya [41] reported a d-spacing ≥30 Å for Ti-PILC. Yuan et al. [42,43] reported delaminated iron-pillared clay and Ti-PILC with a d-spacing of 65.4 Å and 66.4 Å, respectively. Similarly in the present work a large d-spacing of 46 Å was observed in the XRD pattern of Zr-PILC. This unexpected increase in d-spacing might be due to delamination or to some disordered porous structure, rather than to the larger interlayer distance of Zr-PILC [41–43]. In some other reports, however, for the delaminated clay the complete absence of d(0 0 1) peak was also observed [9,10,44].

After doping with vanadia on to the Zr-PILC, the basal spacing remains almost same but a decrease in the intensity can be seen. Impregnation under vigorous stirring of Zr-PILC in vanadia solution induces probably some disorder in the material [45]. This can be also due to a few changes in the structural order of the Zr-PILC after drying and calcinations [38,46].

Fig. 2(a–e) shows the high-angle XRD patterns of fresh Zr-PILC and V/Zr-PILC catalysts. The high-angle XRD pattern of Zr-PILC mainly consists of peak at 2θ of 19.7° and 35° which are assigned to the two-dimensional diffraction ($h\,k$) arising from the random stacking of the clay layers [32]. The peak at 2θ of 28° was a reflection of the crystobalite impurity. It was already reported that no reflections assigned to separate zirconia-containing phases, were observable in Zr-PILCs [47]. The XRD patterns of Zr-PILC after impregnation with vanadia were similar to that of Zr-PILC, and no peak for crystalline vanadium oxides was observed. This suggests that vanadium oxides are well dispersed as nano-crystallites on the Zr-PILC [48,49]. Recently, Bineesh et al. [28] reported that no phases of vanadia were observed in V/Ti-PILC catalyst prepared by impregnation method. Chae et al. [50] also reported that no phases

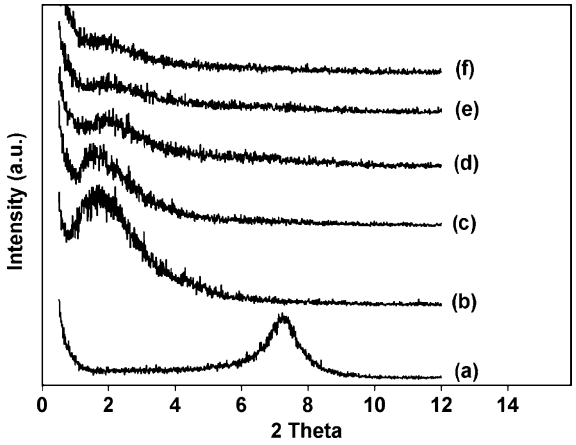

Fig. 1. Low-angle X-ray diffraction patterns: (a) Na-MMT, (b) Zr-PILC, (c) 2 wt.% V/Zr-PILC, (d) 6 wt.% V/Zr-PILC, (e) 11 wt.% V/Zr-PILC, (f) 14 wt.% V/Zr-PILC.

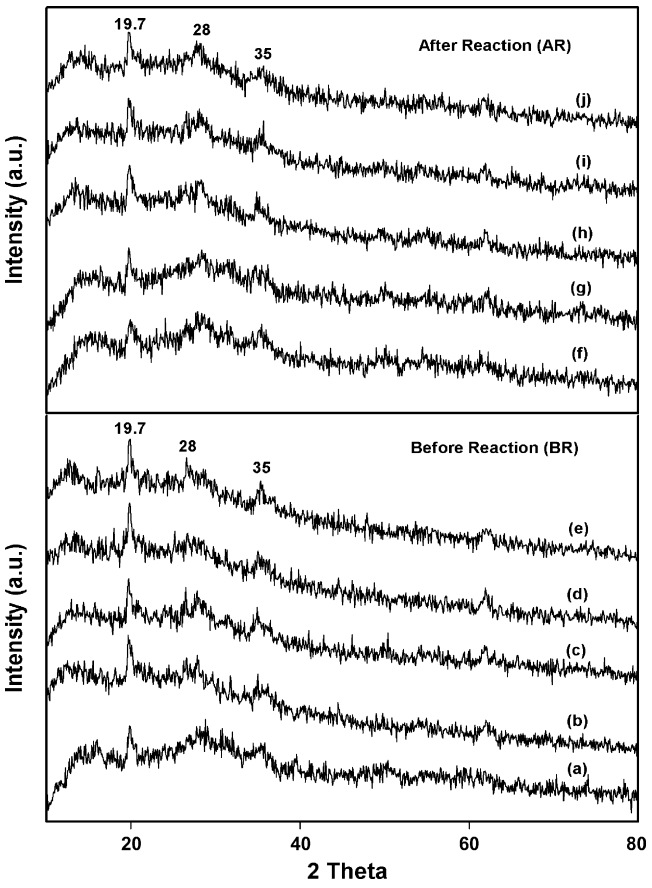

Fig. 2. High-angle X-ray diffraction patterns: (a) Zr-PILC (BR) (b) 2 wt.% V/Zr-PILC (BR), (c) 6 wt.% V/Zr-PILC (BR), (d) 11 wt.% V/Zr-PILC (BR), (e) 14 wt.% V/Zr-PILC (BR), (f) Zr-PILC (AR), (g) 2 wt.% V/Zr-PILC (AR), (h) 6 wt.% V/Zr-PILC (AR), (i) 11 wt.% V/Zr-PILC (AR), (j) 14 wt.% V/Zr-PILC (AR).

Table 2
BET surface area (S_{BET}), total pore volume (V_p), mesopore volume-macropore volume (V_{MP}), micropore volume ($V_{\mu p}$) and acidic properties of the samples investigated.

Samples	S_{BET} (m^2/g)	V_p (cm^3/g)	V_{MP}[a] (cm^3/g)	$V_{\mu p}$ (cm^3/g)	NH_3 (mmol/g)
Na-MMT	26	–	–	–	–
Zr-PILC	281	0.349	0.323	0.026	1.784
2 wt.% V/Zr-PILC	267	0.324	0.315	0.009	1.765
6 wt.% V/Zr-PILC	228	0.287	0.255	0.032	1.710
11 wt.% V/Zr-PILC	184	0.276	0.272	0.004	1.689
14 wt.% V/Zr-PILC	164	0.215	0.205	0.010	1.657

[a] $V_{MP} = V_p - V_{\mu p}$.

of vanadia were observed in V_2O_5/Ti-PILC catalyst below 15 wt.% vanadia calcined at 500 °C.

3.3. Textural properties of Zr-PILC and V/Zr-PILCs

The textural properties of pillared clays mainly depend upon the nature of pillars between the clay sheets, preparation method and the temperature of calcinations. Table 2 shows the textural data obtained from the BET surface area analysis. The BET surface area of Zr-PILC was 281 m^2/g, whereas that of the initial clay was only 26 m^2/g. The large increase in the surface area of Zr-PILC indicates the successful pillaring of ZrO_2 species into the silicate layers of the clay. During the process of pillaring, the expansion in the clay structure and desegregation of the clay particles largely contributes to the enhancement of the surface area and porosity of the clay materials [51]. Samples synthesized from refluxed $ZrOCl_2$ solution were reported to have higher surface areas than those prepared from unrefluxed solutions [14,52]. This might be due to the formation of highly polymerized zirconium species during the process of refluxing. It can be seen from the textural data, that along with micropores, a rather high meso-macroporous volume was revealed in Zr-PILC. These mesopores or macropores appear due to the delamination process occurred in the pillared clay arising from the edge-to-face and edge-to-edge interactions apart from the face-to-face interaction [11,13,47,53]. This result is in good agreement with the broad (0 0 1) reflection with high basal spacing (46 Å) obtained from the XRD.

The high surface area obtained by pillaring allows good vanadia dispersion on the Zr-PILC. However, an increase in the vanadia loading onto the Zr-PILC support resulted in a decrease in surface area and total pore volume, which might be due to pore blockage by progressive filling with vanadia species.

Nitrogen adsorption/desorption isotherms of Zr-PILC and V/Zr-PILCs are shown in Fig. 3A. It can be seen that for Zr-PILC the adsorption/desorption isotherms showed hysteresis loop of type H3 in the IUPAC classification, associated with the presence of slit-like pores in the layered materials [33,42]. Similar shapes of hysteresis loop were observed for Zr-PILC after doping with vanadia, but the height of the hysteresis loop decreased with vanadia loading due to the decrease in the pore volume resulting from the pore blockage [54]. A narrow pore size distribution with mean value around 40 Å calculated from the desorption branch of the isotherm using BJH method is shown in Fig. 3B. It can also be observed that the mean pore diameter is more or less constant after the doping of vanadia on Zr-PILC.

3.4. X-ray photoelectron spectroscopy

The surface oxidation states and binding energy (BE) of vanadium and zirconium were analyzed by XPS. Table 3 shows the binding energies of Zr $3d_{5/2}$ and V $2p_{3/2}$ in the fresh samples. The BE of Zr $3d_{5/2}$ was observed at 182.9 eV for all samples, which corresponds to Zr attached to hydroxyl groups [55]. A binding energy around 517 eV corresponding to V $2p_{3/2}$ was observed for all V/Zr-PILC catalysts. This indicates that most of the vanadium is present mainly in the +5 valence form, probably as V_2O_5 [48,49,56].

Fig. 4(a–d) shows the XPS spectra of V $2p_{3/2}$ for all fresh V/Zr-PILC catalysts. The intensity of the V $2p_{3/2}$ peak increased with increas-

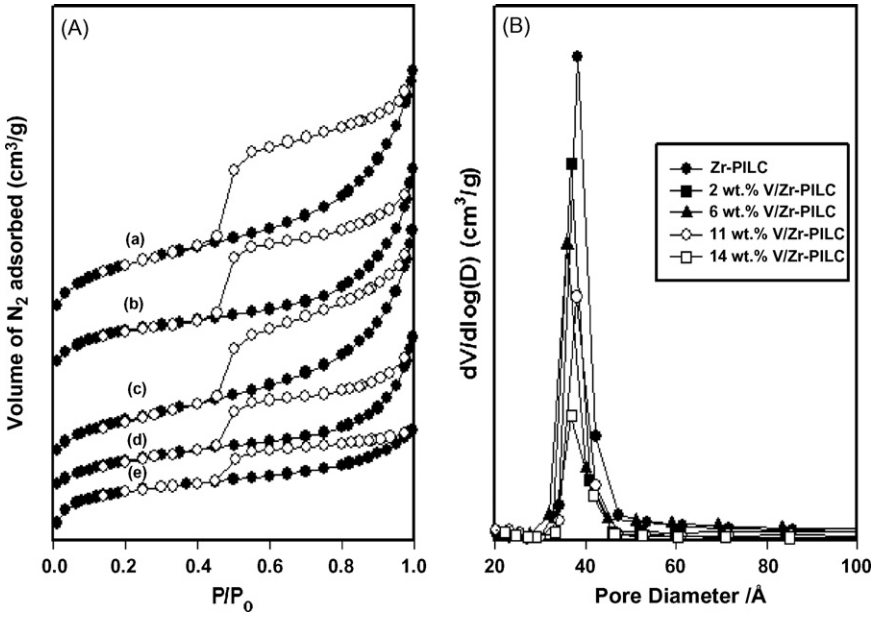

Fig. 3. (A) N_2 adsorption/desorption isotherms of the samples: (a) Zr-PILC, (b) 2 wt.% V/Zr-PILC, (c) 6 wt.% V/Zr-PILC, (d) 11 wt.% V/Zr-PILC, (e) 14 wt.% V/Zr-PILC. (B) Pore size distribution profiles of Zr-PILC and V/Zr-PILC catalysts.

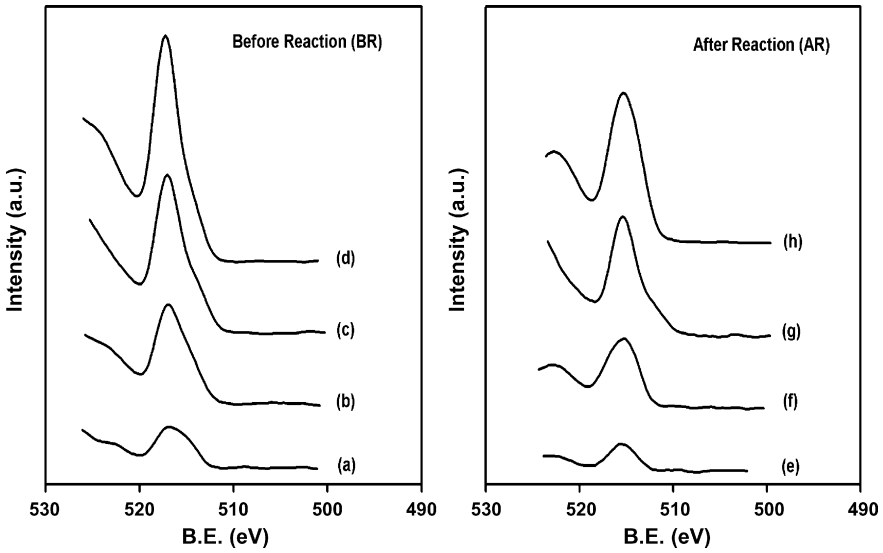

Fig. 4. XPS spectra of V $2p_{3/2}$ of V/Zr-PILC catalysts: (a) 2 wt.% V/Zr-PILC (BR), (b) 6 wt.% V/Zr-PILC (BR), (c) 11 wt.% V/Zr-PILC (BR), (d) 14 wt.% V/Zr-PILC (BR), (e) 2 wt.% V/Zr-PILC (AR), (f) 6 wt.% V/Zr-PILC (AR), (g) 11 wt.% V/Zr-PILC (AR), (h) 14 wt.% V/Zr-PILC (AR).

ing vanadia content on Zr-PILC without any change in peak position. This shows that the vanadium in all loaded catalysts is in +5 oxidation state. Table 3 shows the surface atomic ratios $(V/Zr)_s$ and the corresponding bulk ratios $(V/Zr)_b$. The surface V/Zr ratios are much higher than the bulk V/Zr ratios for 2 and 6 wt.% V/Zr-PILCs, but these ratios were almost similar at 11 and 14 wt.%. This suggests the presence of V_2O_5 crystals on the sample with high vanadia content [49,57].

3.5. ^{51}V solid state NMR

The dispersion and structural features of supported species can depend strongly on the support. Although XPS demonstrated the existence of vanadium on Zr-PILC in the +5 oxidation state it does not provide any evidence for the local environment in the two-dimensional vanadium (V) oxide on the support. Solid-state NMR is a novel and promising approach to examine the local environment of the vanadium at the surface, and provide insight into the types of sites present and their role in the catalytic activity. Furthermore, the ^{51}V nucleus (spin $I = 7/2$) is highly favorable to solid-state NMR because it is in 99.76% natural abundance and has a high receptivity and short spin-lattice relaxation time [50,58,59].

Fig. 5 shows the ^{51}V wide-line NMR spectra for series of V/Zr-PILC catalysts. There are at least three types of signals are visible in the spectra of catalysts with varying intensities depending on the vanadia content. At low vanadia loading, a peak around −620 to −650 ppm was observed, which is mainly due to tetrahedral vanadia species on the catalyst surface. As the vanadia loading increased, the peak shifted to −340 to −360 ppm range, which is generally assigned to distorted octahedral vanadia species [60,61]. The tetrahedral and octahedral vanadia species detected by ^{51}V NMR are mainly monomeric and polymeric vanadia, respectively [62]. For the higher vanadia loading of 11 wt.% and 14 wt.%, a low intensity peak around −1250 ppm was obtained due to the formation of crystalline vanadia with a square pyramidal coordination [59–61,63]. This result is in good agreement with the XPS data. Therefore, the ^{51}V NMR spectra of the catalysts confirm the co-ordination and the dispersion of vanadia over the support.

Table 3
XPS analysis data of the fresh samples.

Catalysts	Binding energy (eV)			
	Zr $3d_{5/2}$	V $2p_{3/2}$	$(V/Zr)_s$[a]	$(V/Zr)_b$[b]
Zr-PILC	182.9	–	0	0
2 wt.% V/Zr-PILC	182.9	517.1	0.21	0.06
6 wt.% V/Zr-PILC	182.9	517.2	0.38	0.16
11 wt.% V/Zr-PILC	182.9	517.1	0.45	0.37
14 wt.% V/Zr-PILC	182.9	517.3	0.50	0.48

[a] Surface atomic ratio.
[b] Bulk atomic ratio.

3.6. Temperature-programmed reduction (H_2-TPR)

The reducibility of the catalysts can be evaluated by H_2-TPR experiment. Fig. 6 shows the TPR profiles of the V/Zr-PILC catalysts calcined at 400 °C. It is well-known that low reduction temperatures correspond to a high degree of vanadia dispersion. It can be seen that TPR profiles showed only single peak irrespective of vanadia loading, which widened and shifted progressively towards high temperature (above 500 °C) as the loading increased to 11 and 14 wt.%, respectively. In general the TPR profile of bulk V_2O_5 exhibits reduction peaks at 655, 686, and 807 °C [57,64]. In our case the observed shift towards high temperature indicates the formation of V_2O_5 crystals. However, the temperature of maximum reduction rate is lower for all samples than that of pure V_2O_5, indicating a

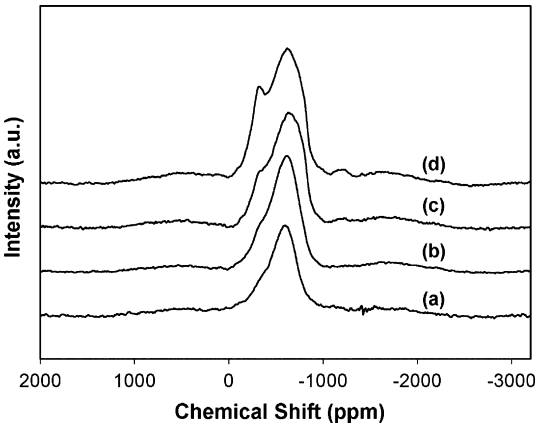

Fig. 5. ^{51}V NMR spectra of V/Zr-PILC catalysts: (a) 2 wt.% V/Zr-PILC, (b) 6 wt.% V/Zr-PILC, (c) 11 wt.% V/Zr-PILC, (d) 14 wt.% V/Zr-PILC.

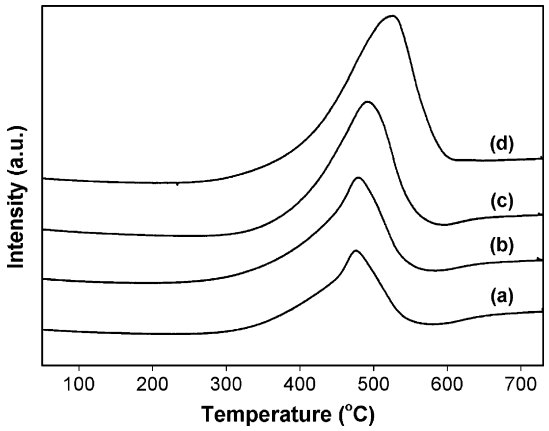

Fig. 6. H_2-TPR profiles of V/Zr-PILC catalysts: (a) 2 wt.% V/Zr-PILC, (b) 6 wt.% V/Zr-PILC, (c) 11 wt.% V/Zr-PILC, (d) 14 wt.% V/Zr-PILC.

significant interaction of crystalline V_2O_5 phase with the support [65]. This behaviour has been explained as due to weakening of the vanadyl group due to the interaction with the vanadia surface. Thus, the variations observed in the reduction peak temperature and peak shape may be interpreted as follows: at low vanadia contents most of the V atoms interact with the Zr-PILC support giving the higher reducibility, but as vanadia loading increases a higher proportion of surface vanadium atoms interacts with internal vanadium layer, so increasing the bond strength of the vanadyl group, approaching it to that of pure V_2O_5. This leads also to a higher heterogeneity of the vanadium reduction centers which causes the widening of the reduction peak [66]. Therefore, it may be concluded that catalyst with higher vanadia contents must have V_2O_5 crystals which is consistent with solid-state ^{51}V NMR and XPS study.

3.7. Temperature-programmed desorption of ammonia (NH_3-TPD)

Fig. 7 shows the NH_3-TPD profiles of Zr-PILC and V/Zr-PILCs. The data is shown in Table 2. The acidity and acid site types (Lewis and Bronsted) depend on the exchanged cations, preparation method and nature of the starting clay [67,68]. In general, the pillaring of clay causes a considerable increase in acidity. This increase arises from exposure of the clay structure and the pillar metal oxide [69]. The acid site desorption pattern could be classified into weak (desorption at 150 °C) and strong (desorption at 600 °C) acid sites. The peak at low temperature is due to ammonia desorption from the weak Bronsted acid sites, while that at high temperature corresponds to the desorbed ammonia from the strong Lewis acid sites.

It is well-known that both Bronsted and Lewis acid sites exist on Zr-PILCs. The peak at low temperature around 150 °C indicates the existence of Bronsted acid sites on Zr-PILC. These may arise from the hydroxyl groups attached to Zr and also from the structural hydroxyl groups in the montmorillonite layer [55]. It is reported that during the calcination process, the ion exchanged Zr-polyhydroxy cation is converted to hydrated ZrO_2 pillars which are positively charged and contribute to the Bronsted acidity of the material [70]. An intense peak was observed at temperature 600 °C, arising from the desorption of ammonia from strong Lewis acid sites due to zirconia pillars [70]. Thus Zr-PILC proved the presence of both Lewis and Bronsted acidities, Lewis acidity being dominant.

The desorption pattern showed a larger increase in the intensity of Bronsted acid sites than that of Lewis acid sites when Zr-PILC is doped with vanadia. This shows a change in the surface acidic properties of Zr-PILC through the introduction of vanadia.

The desorption pattern also shows that the temperature needed to completely desorb the ammonia slightly decreases with increasing vanadia content, which shows that the strength of the acidic sites decreases with increasing vanadia content [71]. The total amount of ammonia desorbed shown in Table 2 also followed the same trend. It decreases continuously with increasing vanadia content.

3.8. Catalytic performance

The catalytic performance of supported vanadia catalysts are strongly affected by the oxidation state and molecular structure of surface vanadia species, which in turn depend upon the nature of support, preparation methods and amount of vanadia content. Fig. 8 shows the catalytic performance of the V/Zr-PILC catalysts for H_2S oxidation with the reactant composition of $H_2S/O_2/He = 5/2.5/92.5$ at GHSV = 10,000 h^{-1}. All V/Zr-PILC catalysts showed a higher level of H_2S conversion than Zr-PILC. It can be seen that for all V/Zr-PILCs catalyst the H_2S conversion increased with increase in temperature. Most of the H_2S was converted to elemental sulfur through selective catalytic oxidation.

The addition of vanadia onto the Zr-PILC increased the catalytic performance. The activity shown by the vanadia supported catalysts depends on the nature of the surface vanadia species as well as on the acid sites present in the catalyst. An increase in H_2S conversion was observed when vanadia loading increased from 2 to 6 wt.%. This may be due to the well dispersion of vanadia in the form of monomeric and polymeric species. This result is in good agreement with the solid-state ^{51}V NMR spectra. Moreover, XPS showed that there is a uniform dispersion of vanadium on the surface of Zr-PILC

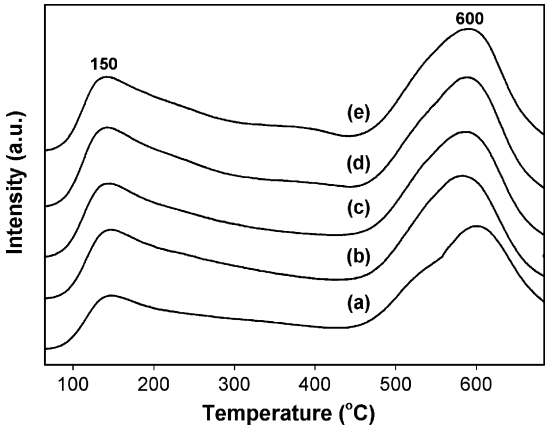

Fig. 7. NH_3-TPD profiles: (a) Zr-PILC, (b) 2 wt.% V/Zr-PILC, (c) 6 wt.% V/Zr-PILC, (d) 11 wt.% V/Zr-PILC, (e) 14 wt.% V/Zr-PILC.

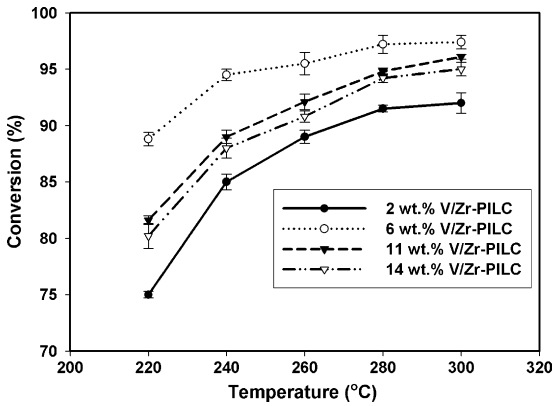

Fig. 8. Conversion of H_2S for V/Zr-PILC catalysts at different temperatures (reactant composition in vol.%: $H_2S/O_2/He = 5/2.5/92.5$, GHSV = 10,000 h^{-1}).

up to 6 wt.%. This indicates that the catalytic performance showed by V/Zr-PILCs depends upon the type of vanadia species present on the support.

The NH_3-TPD results showed that an increase in the intensity of Bronsted acid sites occurred through the addition of vanadia, which might contribute to the catalytic activity. At high temperatures, the presence of strong Lewis acidity may also contribute to the catalytic activity.

A decrease in H_2S conversion was observed at higher vanadia loading of 11 and 14 wt.%. This might be due to the formation of comparatively less reactive crystalline vanadia, which decreases the uniform dispersion of vanadia on the support. The data obtained from the ^{51}V solid-state NMR, XPS and H_2-TPR are in good agreement with this observation. The decrease in catalytic performance at higher loadings can also be explained by the decrease in specific surface area and pore volume caused by pore blockage due to vanadia species (Table 2). Therefore, a change in the dispersion of vanadia species on the surface of support plays an important role in the selective catalytic oxidation of H_2S.

Table 4 shows the selectivity to elemental sulfur at temperatures ranging from 220 to 300 °C for all V/Zr-PILC catalysts. It is interesting to observe that the selectivity remained almost constant around 95–99% for all V/Zr-PILC catalysts, even though the conversion is varied over a wide range. This suggests that the sulfur selectivity of these catalysts is less sensitive to temperature. Yasyerli et al. [22] reported the selective oxidation of H_2S to elemental sulfur over Ce-V mixed oxide at different temperatures (Reaction condition: 1% H_2S, $O_2/H_2S = 0.5$). At 250 °C highest fractional H_2S conversion was obtained with a sulfur yield approaching to unity was reported with Ce-V mixed oxide. No SO_2 formation was observed with a stoichiometric feed composition of O_2/H_2S. But a decrease of the steady state fractional conversion of H_2S, with an increase of temperature over 250 °C was observed. Recently high temperature H_2S sorption activities (Reaction condition: $T = 600$ °C, 2.5% H_2S, 10% H_2 in He) of Ce-Mn mixed oxides and other mixed oxides of Mn were also reported [72]. The H_2S sorption capacity of Ce-Mn (Ce/Mn = 1/3) was found to be higher than the corresponding Zn-Mn, V-Mn, and Fe-Mn mixed oxide sorbents. With V-Mn and Cu-V sorbent it was reported that significant amount of SO_2 formation was detected during the initial stages of the reaction. But with Ce-Mn and Fe-Mn mixed oxides, no SO_2 formation was observed during the sorption of H_2S. Similar results with no SO_2 formation had been reported for other sorbents, such as Mn-Cu and Mn-Cu-V at high temperature [73].

Table 4
Selectivity to SO_2 and S at different temperatures.

Catalyst	Temperature (°C)	S-SO_2 (%)	S-S (%)
	220	0.3	99.7
	240	0.8	99.2
2 wt.% V/Zr-PILC	260	1.5	98.5
	280	1.7	98.3
	300	2.1	97.9
	220	1.5	98.5
	240	3.4	96.6
6 wt.% V/Zr-PILC	260	2.0	98.0
	280	2.3	97.7
	300	2.1	97.9
	220	1.6	98.4
	240	3.7	96.3
11 wt.% V/Zr-PILC	260	4.4	95.6
	280	3.4	96.6
	300	3.4	96.6
	220	0.2	99.8
	240	3.8	96.2
14 wt.% V/Zr-PILC	260	3.0	97.0
	280	2.2	97.8
	300	2.7	97.3

Reaction condition: $H_2S/O_2/He = 5/2.5/92.5$, GHSV = 10,000 h^{-1}, reaction time = 2 h.

The XPS spectra of used V/Zr-PILCs (Fig. 4(e–h)) showed that the peak intensities of V $2p_{3/2}$ were decreased and shifted to lower binding energy (515.6 eV) after the reaction. It indicates that the fresh catalysts having vanadium in the +5 oxidation state is reduced to +4 oxidation state after the reaction. It was already reported that highly oxidized form of vanadium (V^{5+}) produced some amount of SO_2 and partially reduced form of vanadium containing (V^{4+}) was highly selective for the production of elemental sulfur via redox mechanism [27,74]. H_2S is mainly converted to elemental sulfur by reaction (1) and partly to SO_2 by reaction (3). SO_2, which is produced by reactions (2) and (3) can be converted into elemental sulfur by Claus reaction may also give rise to high selectivity. The high-angle X-ray diffraction patterns of used V/Zr-PILCs showed that the phase and shape of the peak was not changed after the reaction (Fig. 2(f–j)). This shows that the bulk structure of the catalysts was not deactivated after the reaction. All these results indicate that V/Zr-PILC catalyst should be very suitable for the industry use to catalyze the oxidation of H_2S to elemental sulfur without considerable SO_2 emission.

The catalytic activity of the support Zr-PILC without vanadia impregnation was performed to determine the influence of the vanadia loading. Zr-PILC showed a very low conversion of approximately 2% at 220 °C which is increased with temperature and reached a maximum of 84% at 300 °C. The activity showed by Zr-PILC at high temperatures might be due to the strong Lewis acid sites present on the ZrO_2 pillars while at low temperatures, the weak Bronsted acid sites arising from the hydrated ZrO_2 pillars and also from the montmorillonite layer may contribute to its activity.

3.9. Effect of O_2/H_2S ratio in the feed stream

We have studied the effect of O_2/H_2S ratio by varying the oxygen concentration in the feed while keeping the H_2S concentration constant at 5 vol.%. In these experiments O_2/H_2S ratio was varied between 0.5 and 2.5. Fig. 9 shows the conversion of H_2S and selec-

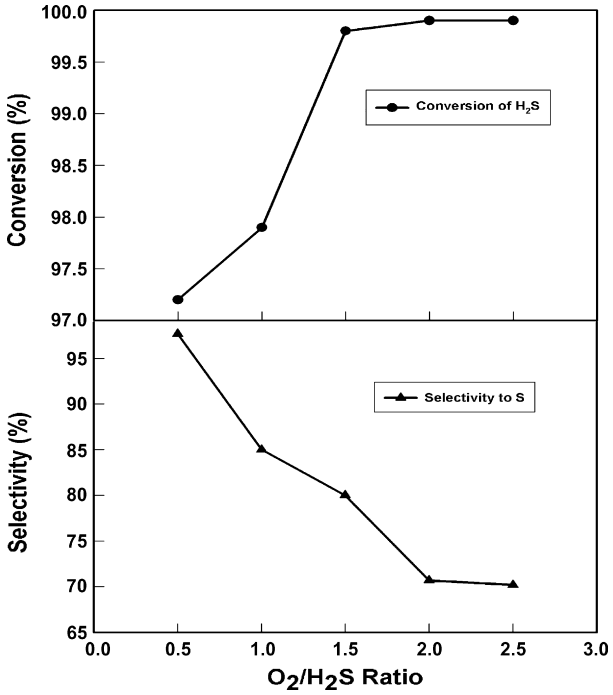

Fig. 9. Effect of O_2/H_2S ratio on conversion and selectivity with 6 wt.% V/Zr-PILC catalyst at 280 °C.

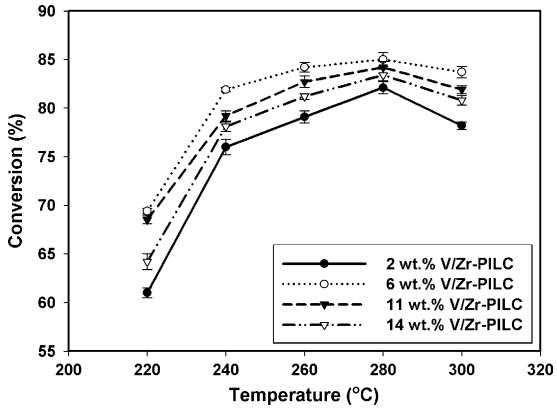

Fig. 10. Effect of water vapor on the conversion of H_2S with V/Zr-PILC catalysts at different temperatures (reactant composition in vol.%: $H_2S/O_2/H_2O/He = 5/2.5/20/72.5$, GHSV = 10,000 h^{-1}).

tivity to sulfur over 6 wt.% V/Zr-PILC at 280 °C. It can be seen that the conversion increased from 97.2% to 99.1% by increasing the ratio of O_2/H_2S from 0.5 to 2.5, while the selectivity to elemental sulfur decreases. It was already reported [22,74,75] that sulfur selectivity decreased with an increase in O_2/H_2S ratio over the stoichiometric value, due to the formation of SO_2. These processes are based on the following irreversible selective oxidation of H_2S to S (reaction (1)) as the main reaction, with other oxidation reactions (reactions (2) and (3)) and the reversible Claus reaction (reaction (4) as side reactions.

As mentioned before, SO_2 which is produced by reactions (2) and (3), can be converted into elemental sulfur by Claus reaction (4). The high selectivity to elemental sulfur can be achieved by suppressing reactions leading to SO_2. An excess of O_2 can lead to the formation of SO_2 according to either the consecutive reaction (2) or parallel reaction (3). In addition, the hydrolysis of the sulfur (reverse Claus reaction) can also produce SO_2. Therefore O_2/H_2S ratio has to maintained in stoichiometry ($O_2/H_2S = 0.5$) in order to decrease SO_2 emission effectively.

3.10. Effect of the water vapor in the reaction stream

As water is an important inhibitor of the Claus catalyst [76], this study investigated the influence of water vapor in the reaction stream under the reactant composition ($H_2S/O_2/H_2O/He = 5/2.5/20/72.5$ at GHSV = 10,000 h^{-1}) for the selective catalytic oxidation of H_2S (Fig. 10). The addition of 20 vol.% water to the feed decreased the conversion of H_2S for all the V/Zr-PILC catalysts. The catalytic performance of 6 wt.% V/Zr-PILC was the highest among all the catalysts. The activity of Zr-PILC support alone showed practically no conversion of H_2S at 220 °C in the presence of 20 vol.% water. This decrease in catalytic activity might due to a competition between H_2S and water vapor for the same active sites of the catalyst. In addition, the decrease in activity may due to the reverse Claus reaction promoted by the addition of water. Simultaneously, selectivity to elemental sulfur was also decreased from 95–99% to 92–93%.

4. Conclusions

The pillaring of clay layers by zirconia resulted in an increase in surface area, which enabled a good dispersion of vanadia species. The catalyst was examined using a variety of characterization techniques to determine the structure and surface properties of vanadia on the support. V/Zr-PILCs showed very good catalytic performance towards H_2S oxidation at 220 to 300 °C. The catalytic performance increased up to a vanadia loading of 6 wt.% due to the high dispersion of vanadia in the form of monomeric and polymeric species. At higher loading of vanadia, there was a decrease in catalytic performance, which was attributed to a decrease in surface area due to the blockage of pores by the vanadia and from the formation of crystalline vanadia. The addition of 20 vol.% water in the reaction stream decreased the level of H_2S conversion and selectivity to elemental sulfur.

Acknowledgements

This study was supported by the Korea Research Foundation (KRF-2008-313-D00201) and Brain Korea 21 program. The authors wish to express their appreciation to the Korea Basic Science Institute.

References

[1] J.A. Lagas, J. Borsboom, P.H. Berben, Oil Gas J. 10 (1988) 68–71.
[2] J. Wieckowska, Catal. Today 24 (1995) 405–465.
[3] R. Kettner, T. Lubcke, N. Liermann, Eur. Patent 0078690 (1983).
[4] R. Kettner, N. Liermann, Oil Gas J. 11 (1982) 63–66.
[5] P.F.M.T. van Nisselrooy, J.A. Lagas, Catal. Today 16 (1993) 263–271.
[6] A. Gil, L.M. Gandia, J.A. Vicente, Catal. Rev. Sci. Eng. 42 (2000) 145–212.
[7] J.T. Kloprogge, J. Porous. Mater. 5 (1998) 5–41.
[8] J.L. Valverde, A.de. Lucas, P. Sanchez, F. Dorado, A. Romero, Appl. Catal. B 43 (2003) 43–56.
[9] J.P. Chen, M.C. Hausladen, R.T. Yang, J. Catal. 151 (1995) 135–146.
[10] T.J. Pinnavaia, M.-S. Tzou, S.D. Landau, R.J. Raythatha, J. Mol. Catal. 27 (1984) 195–212.
[11] M.L. Occelli, Catal. Today 2 (1988) 339–355.
[12] S.L. Jones, Catal. Today 2 (1988) 209–217.
[13] N. Maes, I. Heylen, P. Cool, E.F. Vansant, Appl. Clay Sci. 12 (1997) 43–60.
[14] R. Burch, C.I. Warburton, J. Catal. 97 (1986) 503–510.
[15] S. Moreno, R. Sun Kou, R. Molina, G. Poncelet, J. Catal. 182 (1999) 174–185.
[16] P.R. Pereira, J. Pires, M. Brotas de Carvalho, Langmuir 14 (1998) 4584–4588.
[17] B.G. Mishra, G. Ganga Rao, Micropor. Mesopor. Mater. 70 (2004) 43–50.
[18] K. Ohtsuka, Y. Hayashi, M. Suda, Chem. Mater. 5 (1993) 1823–1829.
[19] K. Bahranowski, R. Grabowski, B. Grzybowska, A. Kielski, E.M. Serwicka, K. Wcislo, E. Wisla-Walsh, K. Wodnicka, Topics Catal. 11/12 (2000) 255–261.
[20] D. Nguyen-Thanh, T.J. Bandosz, J. Phys. Chem. B 107 (2003) 5812–5817.
[21] K.-T. Li, T.-Y. Chien, Catal. Lett. 57 (1999) 77–80.
[22] S. Yasyerli, G. Dogu, T. Dogu, Catal. Today 117 (2006) 271–278.
[23] E.K. Lee, K.D. Jung, O.S. Joo, Y.G. Shul, Appl. Catal. A 284 (2005) 1–4.
[24] N. Keller, C. Pham-Huu, M.J. Ledoux, Appl. Catal. A 217 (2001) 205–207.
[25] T.N. Mashapa, J.D. Rademan, M.J. Janse van Vuuren, Ind. Eng. Chem. Res. 46 (2007) 6338–6344.
[26] V.V. Shinkarev, A.M. Glushenkov, D.G. Kuvshinov, G.G. Kuvshinov, Appl. Catal. B 85 (2009) 180–191.
[27] D.W. Park, B.K. Park, D.K. Park, H.C. Woo, Appl. Catal. A 223 (2002) 215–224.
[28] K.V. Bineesh, D.R. Cho, S.Y. Kim, B.R. Jermy, D.W. Park, Catal. Commun. 9 (2008) 2040–2043.
[29] G.J.J. Bartley, R. Burch, Appl. Catal. 19 (1985) 175–185.
[30] L. Chmielarz, P. Kustrowski, M. Zbroja, W. Lasocha, R. Dziembaj, Catal. Today 90 (2004) 43–49.
[31] H.J. Chae, I.S. Nam, S.W. Ham, S.B. Hong, Catal. Today 68 (2001) 31–40.
[32] L.S. Cheng, R.T. Yang, Microporous Mater. 8 (1997) 177–186.
[33] F. Kooli, W. Jones, Chem. Mater. 9 (1997) 2913–2920.
[34] F. Figueras, A. Mattrod-Bashi, G. Fetter, A. Thrierr, J.V. Zanchetta, J. Catal. 119 (1999) 91–96.
[35] S. Yamanaka, G.W. Brindley, Clays Clay Miner. 27 (1979) 119–124.
[36] G. Fetter, V. Hernandez, V. Rodriguez, M.A. Valenzuela, V.H. Lara, P. Bosch, Mater. Lett. 57 (2003) 1220–1223.
[37] M.R. Sun Kou, S. Mendioroz, V. Munoz, Clays Clay Miner. 48 (2000) 528–536.
[38] J.A. Colin, J.A. de los Reyes, A. Vazquez, A. Montoya, Appl. Surf. Sci. 240 (2005) 48–62.
[39] R. Toranzo, M.A. Vicente, M.A. Banares-Munoz, L.M. Gandia, A. Gil, Micropor. Mesopor. Mater. 173 (1998) 173–188.
[40] T. Mandalia, M. Crespin, D. Messad, F. Bergaya, Chem. Commun. 19 (1998) 2111–2112.
[41] F. Bergaya, J. Porous Mater. 2 (1995) 91–96.
[42] P. Yuan, H.P. He, F. Bergaya, D.Q. Wu, Q. Zhou, J. Zhu, Micropor. Mesopor. Mater. 88 (2006) 8–15.
[43] P. Yuan, X. Yin, H.P. He, D. Yang, L. Wang, J. Zhu, Micropor. Mesopor. Mater. 93 (2006) 240–247.
[44] N. Jagtap, V. Ramaswamy, Appl. Clay Sci. 33 (2006) 89–98.
[45] J. Arfaoui, L.K. Boudali, A. Ghorbel, Catal. Commun. 7 (2006) 86–90.
[46] L. Chmielarz, M. Zbroja, P. Kustrowski, B. Dudek, A. Rafalska-Lasocha, R. Dziembaj, J. Therm. Anal. Cal. 77 (2004) 115–123.
[47] V.A. Sadykov, T.G. Kuznetsova, V.P. Doronin, E.M. Moroz, D.A. Ziuzin, D.I. Kochubei, B.N. Novgorodov, V.N. Kolomiichuk, G.M. Alikina, R.V. Bunina, E.A. Paukshtis, V.B. Fenelonov, O.B. Lapina, I.V. Yudaev, N.V. Mezentseva, A.M.

Volodin, V.A. Matyshak, V.V. Lunin, A.Ya. Rozovskii, V.F. Tretyakov, T.N. Burdeynaya, J.R.H. Ross, Topics Catal. 32 (2005) 29–37.
[48] L.K. Boudali, A. Ghorbel, P. Grange, F. Figueras, Appl. Catal. B 59 (2005) 105–111.
[49] R.Q. Long, R.T. Yang, J. Catal. 196 (2000) 73–85.
[50] H.J. Chae, I.S. Nam, S.W. Ham, S.B. Hong, Appl. Catal. B 53 (2004) 117–126.
[51] B.G. Mishra, G. Ganga Rao, J. Porous Mater. 10 (2003) 93–103.
[52] G.J.J. Bartley, Catal. Today 2 (1988) 233–241.
[53] M.R. Sun Kou, S. Mendioroz, M.I. Guijarro, Thermochim. Acta 323 (1998) 145–157.
[54] K. Soni, B.S. Rana, A.K. Sinha, B. Bhaumik, M. Nandi, M. Kumar, G.M. Dhar, Appl. Catal. B doi:10.1016/j.apcatb.2009.02.010.
[55] S.V. Awate, S.B. Waghmode, K.R. Patil, M.S. Agashe, P.N. Joshi, Korean J. Chem. Eng. 18 (2001) 257–262.
[56] D.A. Bulushev, L. Kiwi-Minsker, V.I. Zaikovskii, A. Renken, J. Catal. 193 (2000) 145–153.
[57] C.L. Pieck, S. de Val, M. Lopez Granados, M.A. Banares, J.L.G. Fierro, Langmuir 18 (2002) 2642–2648.
[58] C. Gheorghe, B. Gee, Chem. Mater. 12 (2000) 682–685.
[59] V. Luca, S. Thomson, R.F. Howe, J. Chem. Soc. Faraday Trans. 93 (1997) 2195–2202.
[60] H. Eckert, I.E. Wachs, J. Phys. Chem. 93 (1989) 6796–6805.
[61] B.M. Reddy, E.P. Reddy, S.T. Srinivas, V.M. Mastikhin, A.V. Nosov, O.B. Lapina, J. Phys. Chem. 96 (1992) 7076–7078.
[62] A.F. Popa, P.H. Mutin, A. Vioux, G. Delahay, B. Coq, Chem. Commun. (2004) 2214–2215.
[63] J.R. Sohn, K.C. Seo, Y.I. Pae, Bull. Korean Chem. Soc. 24 (2003) 311–317.
[64] M.-M. Koranne, J.G. Goodwin Jr., G. Marcellin, J. Catal. 148 (1994) 369–377.
[65] F. Klose, T. Wolff, A. Seidel-Morgenstern, Y. Suchorski, M. Piorkowska, H. Weiss, J. Catal. 247 (2007) 176–193.
[66] H.K. Matralis, Ch. Papadopoulou, Ch. Kordulis, A. Aguilar Elguezabal, V. Cortes Corberan, Appl. Catal. A 126 (1995) 365–380.
[67] M.-Y. He, Z. Lin, E. Min, Catal. Today 2 (1988) 321–338.
[68] H.I. Del Castillo, A. Gil, P. Grange, Catal. Lett. 43 (1997) 133–137.
[69] N.N. Binitha, S. Sugunan, Micropor. Mesopor. Mater. 93 (2006) 82–89.
[70] E.M. Farfan-Torres, E. Sham, P. Grange, Catal. Today 15 (1992) 515–526.
[71] P.H. Mutin, A.F. Popa, A. Vioux, G. Delahay, B. Coq, Appl. Catal. B 69 (2006) 49–57.
[72] S. Yasyerli, Chem. Eng. Process 47 (2008) 577–584.
[73] D. Karayilan, T. Dogu, S. Yasyerli, G. Dogu, Ind. Eng. Chem. Res. 44 (2005) 5221–5226.
[74] S. Yasyerli, G. Dogu, I. Ar, T. Dogu, Chem. Eng. Sci. 59 (2004) 4001–4009.
[75] S.W. Chun, J.Y. Jang, D.W. Park, H.C. Woo, J.S. Chung, Appl. Catal. B 16 (1998) 235–243.
[76] P.H. Berben, Ph.D. Thesis, Univ. of Utrecht, Netherland, 1992.